PHYSICAL REVIEW B VOLUME 48, NUMBER 16 15 OCTOBER 1993-II

Impulse response of the switching charge-density-wave conductor $NbSe_3$

Jeremy Levy and Mark S. Sherwin
Department of Physics and Center for Nonlinear Science, University of California at Santa Barbara, Santa Barbara, California 93106-9530
(Received 16 June 1993)

When a switching charge-density-wave (CDW) conductor is driven with a rectangular voltage pulse, the CDW begins to slide only after a delay τ. We present detailed measurements of the impulse response of the charge-density-wave conductor $NbSe_3$ as a function of the pulse height, temperature, and initial configuration. We find that the average conduction delay $\bar{\tau}$ has an activated temperature dependence for pulse heights sufficiently far above threshold: $\bar{\tau} \propto \exp(E_a/k_BT)$, where $E_a = 24.1 \pm 3.2$ meV, comparable to the CDW gap. We have also performed numerical experiments based on a model which includes the interaction of the CDW with uncondensed electrons. Within this model, we can account for the polarization dependence of the threshold for sliding and the dependence of the conduction delay on the pulse height. If we assume that the ungapped carriers in $NbSe_3$ do not screen the motion of the CDW, then the Arrhenius temperature dependence of the delayed conduction can also be explained. The excellent qualitative agreement between theory and experiment provides a compelling argument that switching behavior arises from the interaction of the CDW with uncondensed carriers.

I. INTRODUCTION

Charge-density-wave (CDW) conductors display a remarkable diversity of nonlinear phenomena.[1] The source of the nonlinearity arises from the interaction of the CDW, commonly treated as an elastically deformable medium,[2] with randomly spaced impurities. The incommensurate CDW is pinned by these impurities, but slides and carries current when an applied electric field exceeds a threshold E_T. At temperatures near the Peierls transition temperature T_P, the threshold is unique and nonhysteretic. At lower temperatures, the interaction of the CDW with thermally excited quasiparticles becomes as important as the interaction with impurities in the semiconducting CDW materials such as $K_{0.3}MoO_3$ and o-TaS_3. Experimental evidence for this includes the observation that the CDW conductivity above threshold becomes proportional to the number of normal carriers[3] and the presence of a broad overdamped mode (associated with internal modes of the CDW) which freezes out at low temperatures.[4] At still lower temperatures a second hysteretic threshold E_T^* develops, above which the CDW slides almost without damping.[5–8]

It has been known for some time that normal carrier screening increases the effective CDW damping,[9] but it was Littlewood who suggested that this interaction might explain the existence of two threshold fields and the hysteretic behavior in the semiconducting materials.[10] Much of the behavior observed in the semiconducting compounds is also seen in $NbSe_3$, which remains metallic at low temperatures. The so-called "switching" behavior, in which the CDW depins suddenly and hysteretically, is observed in some, but not all, samples of $NbSe_3$.[11] Several attempts have been made to understand switching behavior in $NbSe_3$ in terms of phase slip,[12] CDW inertia,[13] and other processes.[11] We have proposed a model[14] similar to Littlewood's and have shown that the uncondensed carriers produce a global coupling term in the equations of motion for the CDW. Current-voltage curves computed from these equations exhibit a single hysteretic depinning transition in one dimension and two threshold fields in two dimensions.[23]

Charge-density-wave dynamics in the switching regime differs markedly from the nonswitching regime; included are the observation of negative differential resistance and related instabilities,[15] anomalously large broadband noise,[15] and period doubling and chaotic behavior in the presence of combined dc and ac fields.[16,17] A particularly unique and puzzling phenomenon was observed by Zettl and Grüner, who found that if one applies a voltage (or current) pulse above threshold, the CDW will begin to slide only after a delay τ.[18] Delayed conduction has also been observed in o-TaS_3.[19]

The phenomenon of delayed conduction provides a stringent test for competing models of switching CDW transport. Joos and Murray[20] proposed an explanation of the results of Zettl and Grüner based on a kinetic Ising model. Strogatz and Westervelt[21] later applied bifurcation theory to several models of switching to make predictions for the dependence of the switching delay on the height of the applied voltage pulse. We showed in a previous paper[22] that, near threshold, the average delay decreases much more steeply with normalized pulse height than predicted by any of the models studied by Strogatz and Westervelt. Furthermore, the distribution of delays displayed a sensitive dependence on the initial configura-

0163-1829/93/48(16)/12223(12)/$06.00 48 12 223

tion, and the delays varied over five orders of magnitude for identical external parameters. The sensitive dependence on initial configuration was not predicted by previous models. Wiesenfeld and co-workers[24,25] showed later that such a sensitive dependence arises naturally in an extension of the Fukuyama-Lee-Rice model with nonuniform impurity strength and the possibility of phase slip.

In this paper, we present the main results of a detailed experimental and numerical study of the phenomena of conduction delays in CDW's. In Sec. III, we describe experiments which have investigated the phenomenon of conduction delays as a function of temperature, pulse height, and initial configuration. Our main results are as follows: Near the threshold for sliding, we observe a broad distribution of "long" delays τ, whose standard deviation exceeds the average, and whose average $\bar{\tau}$ depends quite strongly on the pulse height. As the pulse height is increased there is a distinct crossover to "short" delays, in which the standard deviation is below the average. The short delays decrease approximately exponentially with pulse height. The delay at the crossover between long and short delays (or the delay for a fixed fraction above threshold) displays an Arrhenius temperature dependence with an activation energy E_a comparable to previous measurements of the CDW gap. The switching time t_{sw} (defined as the time taken for the CDW current to rise from 10% to 90% of its asymtotic value) displays a similar temperature dependence. We have also performed experiments in which the initial configuration was prepared in specific ways. The first method involved heating the CDW crystal above the Peierls transition and allowing it to cool in zero field. The second method involved applying a negative pulse to the CDW. In both cases, we observed a lower threshold for sliding when a positive pulse was applied starting from the relaxed configuration.

In Sec. IV, we describe numerical "experiments" on delayed conduction. The model we simulate is a variant of the model of switching and nonswitching CDW transport discussed in Ref. 14. In this variant, both the interaction between the CDW and normal carriers and the nonuniform spatial distribution of impurities are taken into account, but phase slip is ignored. We observe delayed conduction and explain its origin in the model. We find good qualitative agreement with the surprising experimentally observed dependence of conduction delays on initial conditions and pulse height. If we assume that the ungapped carriers in $NbSe_3$ do not screen the motion of the CDW, then the model is also consistent with the observed Arrhenius temperature dependence of the conduction delays τ and switching time t_{sw}. The agreement between experiment and theory provides strong support for the model. The surprising implication, that ungapped carriers in $NbSe_3$ play a negligible role in screening CDW deformations, is an interesting topic for further study.

II. EXPERIMENTAL METHODS

The experiments were performed on three samples of $NbSe_3$ at temperatures 18 K $< T <$ 33 K. All three samples displayed a single, clean switch. In this paper, we will present mostly the results for a single sample, but will summarize the results for the other samples where appropriate.

The samples were grown by conventional vapor transport methods. Switching samples of $NbSe_3$ generally are obtained in freshly grown batches, but we have found that cooling the samples in liquid nitrogen and/or storing them in vacuum greatly prolongs the life of a switching batch. The samples were placed inside of a conflat flange filled with 1 atm of helium gas, in order to minimize Ohmic heating of the sample, and cooled using a closed-cycle helium refrigerator. The samples were mounted in a two-probe configuration on a ceramic 50-Ω microstripline terminated by 50-Ω resistors at each end. The conflat flange can hold up to six samples at a time, which was important because the success rate in finding high-quality samples is quite low. Temperature stability was somewhat problematic, because of the uneven cooling power of the refrigerator, but this difficulty was overcome by using two pairs of temperature sensors and heaters, one near the cold head and one inside the conflat flange. With this method we were able to achieve a temperature stability of ± 10 mK over an indefinite range of time. The samples were driven by a pulse generator with a rise time of 5 nsec.

III. EXPERIMENTAL RESULTS

At temperatures near the Peierls temperature T_{P2}=59 K, the CDW depins smoothly at a threshold E_t. As the temperature is lowered, the CDW conductivity

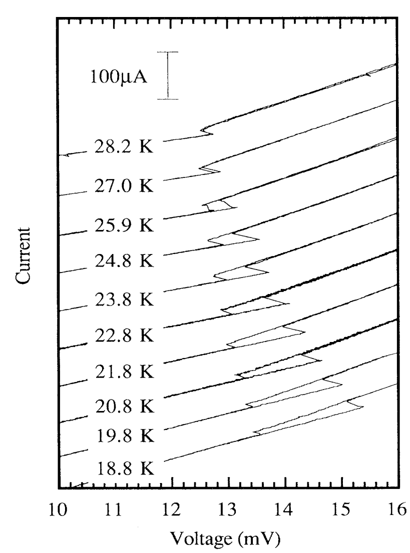

FIG. 1. I-V curves at various temperatures for sample 1 (length is 0.4 mm; Ohmic resistance is 32 Ω at T=20 K). The onset of hysteresis occurs near 28 K, although the I-V curve is double valued at higher temperatures due to the finite impedance of the voltage source. The transitions to and from the sliding states are not vertical, due to the 50-Ω impedance of the voltage source and the 50-Ω terminating resistors. As the temperature is lowered, the Ohmic (low-field) resistance decreases and the hysteresis increases.

near E_t decreases, and a second threshold develops at a higher field E_t^*. This threshold becomes hysteretic, and the width of the hysteresis loop increases as the temperature is lowered further. Figure 1 shows the current as a function of the voltage drop across the sample for sample 1, at temperatures ranging from 28.2 K down to 18.8 K. Due to the low impedance of the sample (32 Ω at T=20 K), the voltage across the sample differs in the sliding and pinned state. The width of the hysteresis loop increases as the temperature is lowered. The Ohmic resistance of the sample decreases with temperature in this range, whereas the sliding state conductivity is approximately independent of temperature.

In the first set of experiments, a 1-sec voltage pulse V_p was applied to the sample, followed by a 2-sec interval with zero voltage, as depicted in Fig. 2. The CDW current was digitized over the range 0.1 μsec–1 sec, and the delay τ was determined by a computer algorithm. The switching time t_{sw} was also measured from the resulting

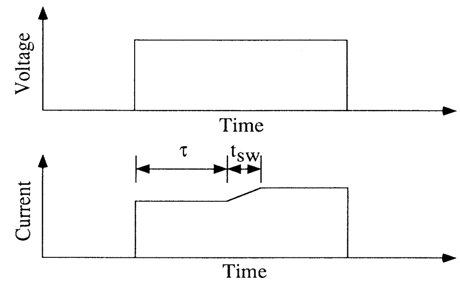

FIG. 2. Schematic representation of the impulse response experiments. The sample is driven by a 1-sec voltage pulse of height V_p, followed by a 2-sec wait period. The CDW current is then digitized, and the conduction delay τ and switching time t_{sw} are determined from the current trace. The experiment is repeated 1024 times for various values of V_p and at different temperatures.

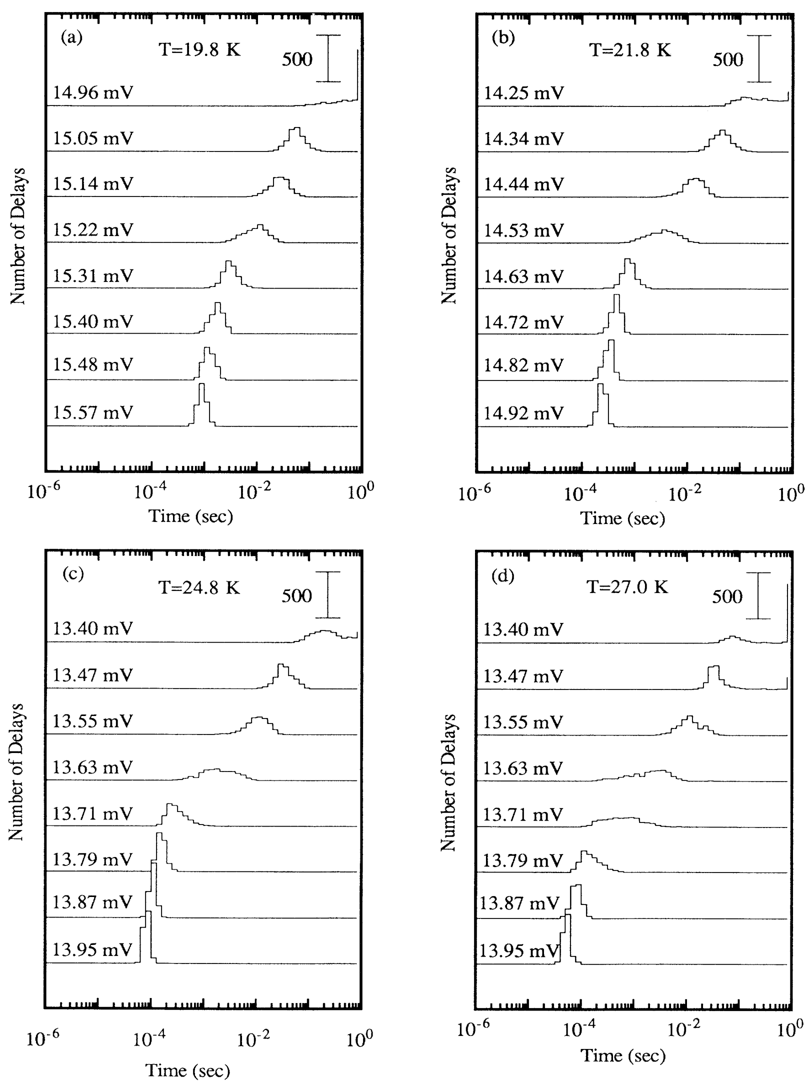

FIG. 3. Distribution of delays as a function of V_{pulse} and temperature for sample 1. For V_{pulse} close to the threshold for sliding, the distribution of delays is broad. As V_{pulse} increases, there is a crossover to a much narrower distribution. (a) T=19.8 K. (b) T=21.8 K. (c) T=24.8 K. (d) T=27.0 K.

current trace. Typically, 1024 delays were measured for a given V_p and temperature.

A. Distribution of delays

Figures 3(a)–3(d) show a histogram of the conduction delays for various temperatures T and pulse heights V_p. The various histograms are offset for clarity. We define as threshold $V_{\rm th}$ the pulse height for which half of the pulses do not result in CDW conduction. Our main results do not depend critically on this choice for $V_{\rm th}$. For T=19.8 K, $V_p^{\rm th}$=14.96 mV, as seen in the top trace of Fig. 3(a). As V_p is increased, the distribution remains broad, but begins to narrow relative to its average near V_p=15.31 mV. Above this pulse height, the distribution remains narrower and the average decreases much less rapidly. Similar behavior is observed in Figs. 3(b)–3(d).

The crossover from a fairly broad distribution to a much more narrow one can be seen more clearly if one looks at the average delay $\bar{\tau}$ and standard deviation σ as a function of V_p. Figures 4(a)–4(c) show the average delay and standard deviation versus the reduced pulse height $\epsilon \equiv (V_p - V_p^{\rm th})/V_p^{\rm th}$ for the three samples which were studied. For values of ϵ below a sample- and temperature-dependent crossover value $\epsilon_{\rm co}$, the distribution of "long" delays is quite broad and the average delay $\bar{\tau}$ depends sensitively on ϵ. Associated with $\epsilon_{\rm co}$ is a fairly distinct crossover at time $\tau_{\rm co}$ to "short" delays, in which $\bar{\tau}$ depends much more weakly on V_p and for which the standard deviation σ is much smaller than $\bar{\tau}$. This crossover time is more pronounced in samples 2 and 3 than in sample 1. The dependence of the short delays on ϵ can be fit fairly well to a power law $\bar{\tau} \propto \epsilon^{-\delta}$ with $\delta \approx 2$

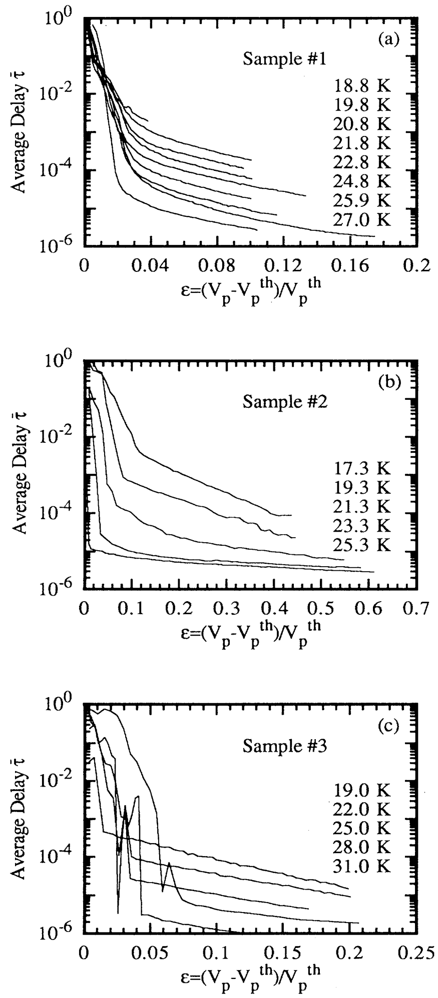

FIG. 4. Plot of average switching delay $\bar{\tau}$(□) and standard deviation σ(△), for samples 1–3, respectively. Near threshold, the delays are "long": $\bar{\tau}$ depends strongly on the reduced pulse height ϵ and the standard deviation σ on the order of $\bar{\tau}$. At larger ϵ, the delays become "short": the standard deviation falls below the average and the dependence of τ on $V_{\rm pulse}$ is much weaker. There is a fairly well-defined crossover time $\tau_{\rm co}$ which separates the two regimes. (a) Sample 1. (b) Sample 2 (length is 0.6 mm). (c) Sample 3 (length is 1.2 mm).

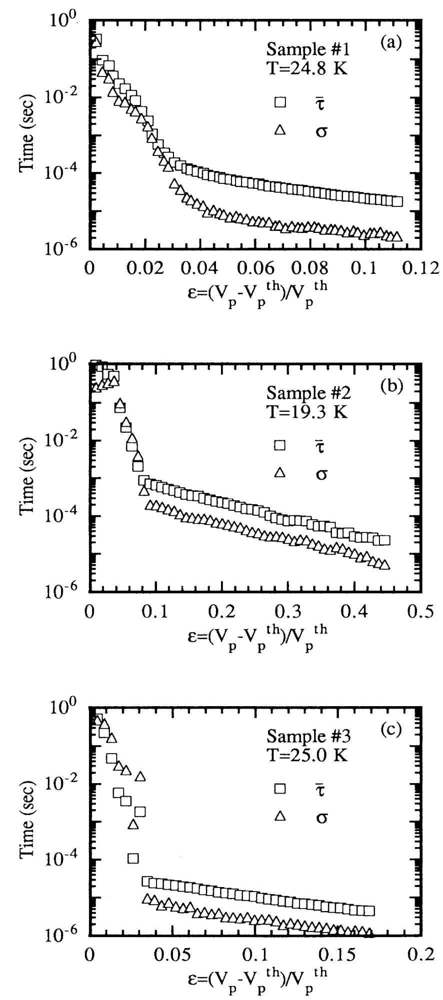

FIG. 5. Average switching delay $\bar{\tau}$ (in seconds) versus ϵ for different temperatures. The delays decrease monotonically as the temperature is increased. (a) Sample 1. (b) Sample 2. (c) Sample 3.

for sample 1, but samples 2 and 3 clearly appear to fit an exponential form much better.

B. Temperature dependence of delays

The conduction delays display a very strong dependence on temperature. By changing the temperature over a few degrees, the average delay can change by several orders of magnitude. Figures 5(a)–5(c) show the average delay $\bar{\tau}$ versus reduced pulse height ϵ at various temperatures for samples 1–3, respectively. As the temperature is increased, the average delay decreases. The temperature dependence of ϵ_{co} is very much sample dependent, remaining essentially constant for sample 1, decreasing with temperature for sample 2, and apparently increasing for sample 3. These sample-to-sample variations may have to do with the fact that the distribution of delays is bimodal in many samples;[22] the presence of only a small fraction of "long delays" may overwhelm an otherwise smaller average, as is the case for Fig. 5(c) at T=31.0 K. The exponential dependences of $\bar{\tau}$ on ϵ seen in samples 2 and 3 are more robust at lower temperatures, becoming less dependent on ϵ as $\bar{\tau}$ approaches a critically small value (3 μsec for sample 2).

The switching time t_{sw} displays a similar dependence on temperature. Figure 6 shows typical short switches for sample 1 at four different temperatures, for values of ϵ slightly above ϵ_{co}. As the temperature is increased from 19.8 K to 27.0 K, τ decreases by more than two orders of magnitude. The switching time t_{sw} decreases in a similar fashion. The switching time t_{sw}, while highly dependent on temperature, displays no observable dependence on ϵ.

The temperature dependence of both $\bar{\tau}_{co}$ and t_{sw} are shown in Figs. 7(a) and 7(b). Figure 7(a) shows an Arrhenius plot of τ_{co} versus inverse temperature for three

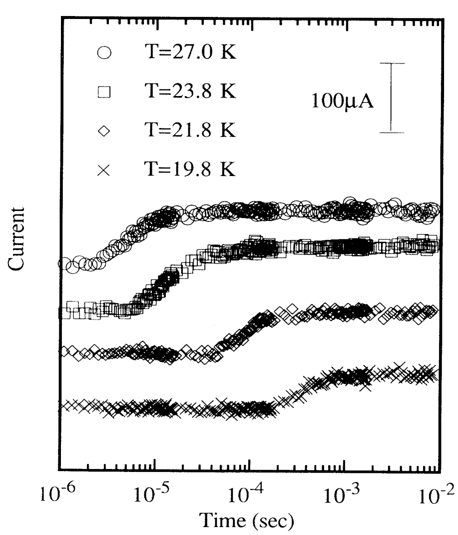

FIG. 6. Experimentally measured CDW current versus time for a typical short delay at four different temperatures. The four traces are offset vertically for clarity. Note that the time scale for both τ and t_{sw} scale together (i.e., the curves look similar but shifted on a logarithmic scale).

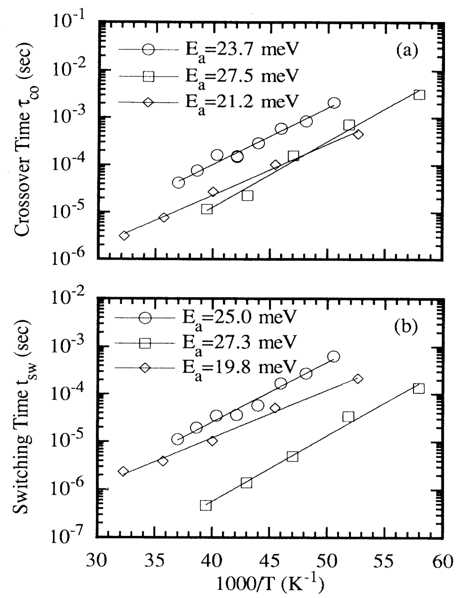

FIG. 7. (a) Plot of crossover time τ_{co} versus inverse temperature for three different samples of $NbSe_3$. The solid lines represent fits to the form $\tau_{co} \propto \exp(E_a/k_BT)$. (b) Plot of switching time t_{sw} for the same samples as in (a). Solid lines are fits to the same functional form as in (a).

different samples. The data are clearly fit well by straight lines, with a mean activation energy $E_a = 24.1\pm3.2$ meV. The switching time t_{sw} also appears to behave in an activated fashion (with mean activation energy $E_a = 24.0 \pm 3.8$ meV), as shown in Fig. 7(b). The activation energy is comparable (i.e., within factors of 2) to more direct measurements of the CDW gap,[26–28] as well as measurements of the activated behavior of the CDW current in $NbSe_3$ below E_T^* by Adelman *et al.*[29]

C. "Melting" the CDW

We have also performed experiments in which we prepared the initial configuration of the CDW in various ways. One method that we have used previously[22] involves applying a sinusoidal signal to the CDW of the form $V(t) = V_0(\frac{1}{2})(1 - \cos\Omega t)\cos(2\pi f t)$, where $2\pi/\Omega =$ 3 sec and f ranged from 100 Hz to 100 kHz. The disadvantage of this method of preparing the initial configuration is that one has little intuition of what the final configuration of the sample might be, and there is no guarantee that the configuration will be the same for every pulse. A conceptually simpler method of preparing the initial configuration is the following: first, the sample is heated above the Peierls temperature, in effect "melting" the CDW. Next, the sample is allowed to cool slowly at zero electric field, to a final temperature. The CDW should then be in a highly reproducible configuration, and one can investigate the impulse response beginning from this configuration. Several 1-sec pulses are then applied as in the earlier experiments.

Figure 8 shows the time evolution of the current for two successive pulses (pulse 1 and pulse 2) at various values of V_p and $T = 20$ K for sample 1. The initial configuration of the CDW was prepared as described above. The traces for different values of V_p are offset for clarity, but there is no offset between pulse 1 (squares) and pulse 2 (circles). The top two traces show the current versus time for V_p=14.14 mV. At the end of both pulses the CDW remained in the pinned state. For pulse 1, there is a large polarization current, which appears to decay abruptly near 30 μsec and disappear completely by 10 msec. This polarization current is not observed for pulse 2. At V_p=14.19 mV, one sees a similar polarization current for pulse 1 and the CDW remains in the sliding state. After approximately 100 μsec, even though there is no clear switch, the current has reached an approximately steady state with the CDW sliding. The second pulse shows no polarization current and remains in the pinned state. Similar behavior is also observed at V_p=14.73 mV, although the time at which the polarization current decreases has decreased. At V_p=15.00 mV, one observes delayed conduction in pulse 2 at 100 msec. The conduction delay shortens as V_p is increased to 15.45 mV, consistent with earlier experiments. The response to pulse 2 and successive pulses is qualitatively indistinguishable from the response of the CDW when its initial condition was not specially prepared.

The initial configuration of the CDW appears to have a profound effect on the pulse-driven threshold for sliding. Figure 9 shows a plot of the total current through the sample at the end of the first and second pulses versus V_p.

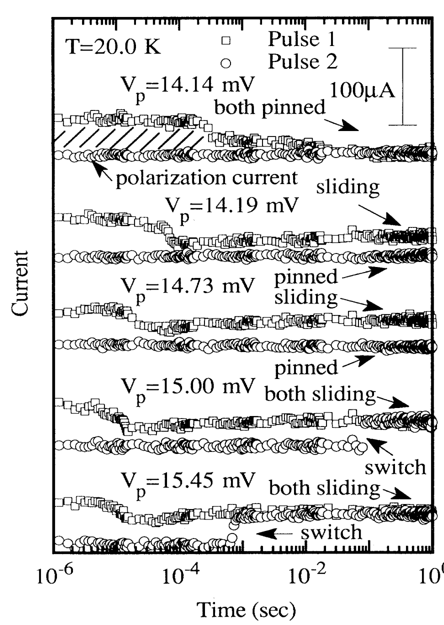

FIG. 8. Current versus time for various values of V_p, for two different initial conditions. Pulse 1 (□) is the response after heating the sample to 70 K and cooling down to 20 K over a period of 600 sec. Pulse 2 (○) started 3 sec after the end of pulse 1. The current traces for different $V_{\rm pulse}$ are shifted for sake of clarity. See text for a detailed description.

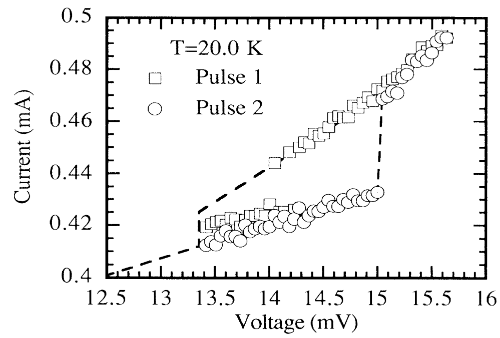

FIG. 9. Final current versus pulse height V_p for two successive pulses (1 and 2) after heating the sample above the Peierls temperature ($T \approx$70 K) and allowing it to cool to $T = 20$ K at zero field. The dashed line represents the I-V curve for slow ramping. The threshold for switching is significantly lower for the first pulse.

The dashed line indicates the hysteresis loop obtained from a slowly ramped I-V trace. For pulse 1, the CDW slides when V_p is near the middle of the hysteresis loop, while for pulse 2 and successive pulses, the CDW slides only if V_p exceeds the threshold obtained from the slowly ramped I-V curve.

The polarization currents described above, as well as the polarization dependence on the threshold for sliding, were reproduced in sample 2 and were not checked for sample 3. However, sample 2 displayed a clear "switch" into the sliding state even in response to the first pulse after "melting."

D. "Depolarizing" the CDW

A similar experiment was performed in which the CDW was prepared by a 1-sec pulse of strength $V_{\rm dep}$, followed by 2 sec at zero bias. Several 1-sec pulses were then applied as in the earlier experiments. Figures 10(a) and 10(b) show current traces for two values of $V_{\rm dep}$. As in Fig. 8, the traces for different values of V_p are offset for clarity, but there is no offset between pulse 1 (squares) and pulse 2 (circles). In Fig. 10(a) $V_{\rm dep} = -4.18$ mV. At $V_p = 14.87$ mV, there are no measurable polarization currents for pulse 1, in contrast to the behavior for Fig. 10. As V_p is increased, we observe no statistically significant difference between pulse 1 and pulse 2. At $V_p = 14.95$ mV, switching occurs for pulse 1, but not for pulse 2, while at $V_p = 15.05$ mV, the situation is reversed. At $V_p = 15.23$ mV, both pulse 1 and pulse 2 produce a switch at almost exactly the same time.

The situation is different when the magnitude of $V_{\rm dep}$ is increased to -8.36 mV, as shown in Fig. 10(b). The current traces are essentially the same for both pulse 1 and pulse 2 at $V_p = 14.23$ mV. At $V_p = 14.32$ mV switching occurs for pulse 1, but not for pulse 2. At $V_p = 15.05$ mV both pulse 1 and pulse 2 produce switching, although one can see that the delay is much longer for pulse 2. The

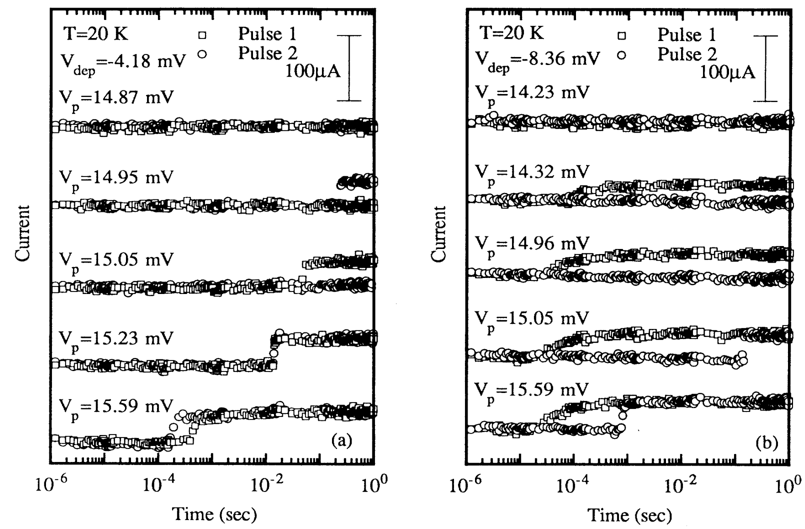

FIG. 10. (a) Current versus time for two successive pulses [1 (□) and 2 (○)] at various values of V_{pulse}, after a 1-sec depolarizing pulse of strength V_{dep}. (a) $V_{\mathrm{dep}} = -4.18$ mV. (b) $V_{\mathrm{dep}} = -8.36$ mV.

switching time t_{sw} is approximately the same for both pulses.

Figures 11(a) and 11(b) show plots of the total current through the sample at the end of the first and second pulses versus V_p for the two values of V_{dep} corresponding to Figs. 10(a) and 10(b), respectively. The dashed line indicates the hysteresis loop obtained from a slowly ramped I-V trace. In Fig. 11(a), there is no appreciable difference between pulse 1 and pulse 2, while Fig. 11(b) clearly shows that the threshold for switching is somewhere near the middle of the hysteresis loop for pulse 1 and near the threshold for the slowly ramped I-V curve for pulse 2 and successive pulses. Behavior similar to Fig. 11(b) was observed for higher values of V_{dep}, with no appreciable change in the threshold for pulse 1. For pulse 1, the CDW slides when V_p is near the middle of the hysteresis loop, while for pulse 2 and successive pulses, the CDW slides only if V_p exceeds the threshold obtained from the slowly ramped I-V curve.

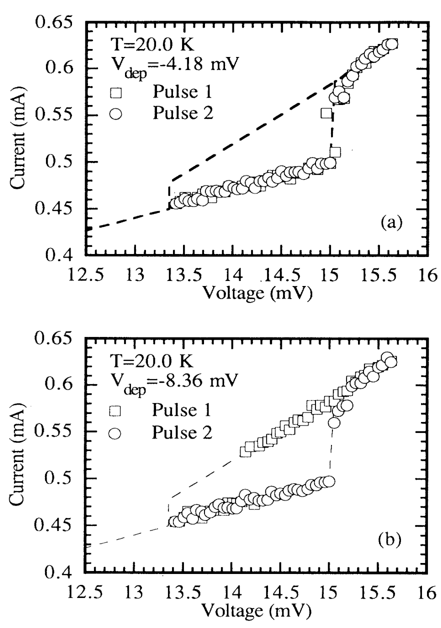

FIG. 11. Final current versus pulse height V_p for pulse 1 and pulse 2 for depolarizing experiment (see Fig. 10). Dashed line shows hysteretic I-V curve for slowly swept voltage. The voltage shown assumes that the response of the sample is ohmic (cf. Fig. 1). (a) $V_{\mathrm{dep}} = -4.18$ mV. There is little difference between pulse 1 and pulse 2. (b) $V_{\mathrm{dep}} = -8.36$ mV. Pulse 1 ends up in the sliding state for $V_{\mathrm{pulse}} > 14.2$ mV, whereas the threshold is $V_{\mathrm{pulse}} > 15.0$ mV for pulse 2.

IV. NUMERICAL RESULTS

A. Previous work

Several theories have been proposed to explain CDW conduction in switching samples. Hall, Hundley, and Zettl[30] have proposed that switching samples contain a few "ultrastrong pinning centers,"[31] which prevent the intact CDW from sliding. The CDW can slide only when the internal strains become sufficiently large to cause tears, or phase slips, in the fabric of the condensate. Inui *et al.*[12] proposed a many-body Hamiltonian embodying these ideas, and they numerically investigated a one-degree-of-freedom version. Strogatz *et al.*[32] have proposed a different, exactly soluble many-body Hamiltonian that is isomorphic to the mean-field x-y model. Each of these models shows delayed switching,[21] and there has not been much experimental work that could distinguish between them. Other mechanisms have also been proposed to explain delayed conduction specifically.[18,20,33,34] In this section, we discuss a variant of the model described in Ref. 14, in which the distribution of impurities has been taken into account. We then present numerical simulations and compare our results with experiment.

B. Equations of motion

We first discuss the origin of the equations of motion that we use for our simulations. We have found that it is crucial to employ a nonuniform (Poisson) distribution of impurity spacings, because it is this distribution which gives rise to polarization-dependent effects such as the pulse-sign memory effect.[35] Our method of discretization differs slightly (but significantly) from previous methods.[36,35] We start as usual with the Fukuyama-Lee-Rice energy functional:

$$U = \int dx\, \frac{K}{2}\left[\frac{\partial \phi}{\partial x}\right]^2 - \phi E(x) + \sum_j \rho(x) V(x - x_j), \tag{4.1}$$

where $\phi(x)$ is the CDW phase as position x, K is the CDW elasticity, $E(x)$ is the (local) electric field, $\rho(x)V(x) \approx -\cos[Qx + \phi(x)]\delta(x)$ is the impurity energy associated with impurity site x_j, and Q is the CDW wave vector. We then make the ansatz that the system is overdamped, with a damping constant γ_0. The overdamped equation of motion arises from the equation

$$\gamma_0 \dot{\phi}(x) = -\frac{\delta U}{\delta \phi(x)}. \tag{4.2}$$

We then integrate Eq. (4.2) between impurity sites, making the following *approximations*:

$$\int_{s_j}^{s_{j+1}} dx\ \phi(x) \approx (s_{j+1} - s_j)\ \phi(x_j) \equiv d_j \phi_j\ , \tag{4.3a}$$

$$\int_{s_j}^{s_{j+1}} dx \sin[Qx + \phi(x)]\delta(x - x_j) = \sin[\phi(x_j) + Qx_j] \approx \sin[\phi_j - \beta_j]\ , \tag{4.3b}$$

$$\int_{s_j}^{s_{j+1}} dx \frac{\partial^2 \phi}{\partial x^2} = \left[\frac{\partial \phi}{\partial x}\right]_{s_j}^{s_{j+1}} \approx \frac{\phi_{j+1} - \phi_j}{x_{j+1} - x_j} - \frac{\phi_j - \phi_{j-1}}{x_j - x_{j-1}} \equiv \Delta\phi_j\ , \tag{4.3c}$$

$$\int_{s_j}^{s_{j+1}} dx\ E(x) \approx d_j\ E(x_j) \equiv d_j\ E_j, \tag{4.3d}$$

where $s_j = (x_{j-1} + x_j)/2$ and $\beta_j \equiv -Qx_j$. (If the average impurity spacing is much larger than the CDW wavelength, then the β_j can be considered to be random numbers modulo 2π.) The discrete equations of motion then become[37]

$$\gamma_0 d_j \dot{\phi}_j = K\Delta\phi_j - \sin(\phi_j - \beta_j) + d_j E_j(t). \tag{4.4}$$

The CDW current density J_{CDW} coexists with a normal current density j_N, which together form an incompressible fluid:

$$\nabla j = \frac{dJ_{\text{CDW}}}{dx} + \frac{dJ_{\text{N}}}{dx} = 0, \tag{4.5}$$

where $J_{\text{CDW}}(x) = \dot{\phi}(x)$ and $J_{\text{N}}(x) = E(x)/\gamma_1$. Here γ_1 is the resistance of the uncondensed carriers which are excited across the CDW gap at finite temperature. Condition (4.5) implies that the total current obeys the condition

$$J(x) = \frac{1}{L}\int_0^L dx\ J(x), \tag{4.6}$$

where $L = \sum_{j=1}^{N} d_j$ is the length of the CDW. The discrete version of Eq. (4.6) is the following:

$$\dot{\phi}_j + \frac{E_j}{\gamma_1} = \frac{1}{L}\sum_{k=1}^{N} d_k\left(\dot{\phi}_k + \frac{E_k}{\gamma_1}\right) \equiv \langle\dot{\phi}_k\rangle_k + \frac{E}{\gamma_1}. \tag{4.7}$$

If one substitutes for $d_j E_j$ using Eq. (4.7), then Eq. (4.4) becomes

$$(\gamma_0 + \gamma_1) d_j \dot{\phi}_j = K\Delta\phi_j - \sin(\phi_j - \beta_j) + d_j E(t) + \gamma_1 d_j \langle\dot{\phi}_k\rangle_k. \tag{4.8}$$

C. Numerical experiments

We have studied the impulse response of Eq. (4.8) as a function of γ_1/γ_0 and initial configuration, in analogy with the experiments described in Sec. III. We chose a system of size $L = N = 64$, with $K = 0.1$. Periodic boundary conditions were employed. Time was measured in units of γ_0, which was set to $\gamma_0 = 1$ in all the computations. We looked at a single distribution of impurities x_j, and we do not expect the general results to depend critically on the exact distribution. Our aim was to reproduce qualitatively the striking features of our experiments on delayed conduction. We have not attempted to make a quantitative comparison of experiment and theory, although such a comparison is in principle possible. We have concentrated on features of our results which appear robust in the three samples which we have examined.

In the first set of numerical experiments, we applied a time-dependent field $E(t)$ of the form

$$\begin{aligned} E(t) &= 0, \qquad && t < 0 \\ E(t) &= E_p, && t \geq 0, \end{aligned} \tag{4.9}$$

starting from two different initial configurations, as shown in Fig. 12(a). Configuration 1 was obtained by setting all of the phases ϕ_j to zero and allowing the CDW to relax into a metastable state. Configuration 2 was obtained by allowing the final configuration of one of the first pulses with $E_p = 0.523$ to relax at zero field. Figure 12(b) shows the CDW current as a function of time for two different values of E_p and $\gamma_1 = 10$, starting from configuration 1. For $E_p = 0.523$, the CDW polarizes, but does not switch. The CDW switches for $E_p = 0.524$, and the delay changes from $\tau = 270$ to $\tau = 240$ when E_p is increased to $E_p = 0.525$. Figure 12(c) shows the CDW current as a function of time for two different values of E_p and $\gamma_1 = 10$, starting from configuration 2. When the CDW starts in a highly polarized state, the polarization currents become much smaller and the switching delays much longer. For $E_p = 0.585$, the CDW polarizes somewhat but does not switch. For $E_p = 0.586$, the CDW switches near $t = 700$, more than three times longer than near threshold in the unpolarized case (note the change of time scale). The dependence of τ on E_p is also more pronounced for configuration 2. The pulse for which $E_p = 0.587$ switches near $t = 475$, a much larger fractional change than for configuration 1.

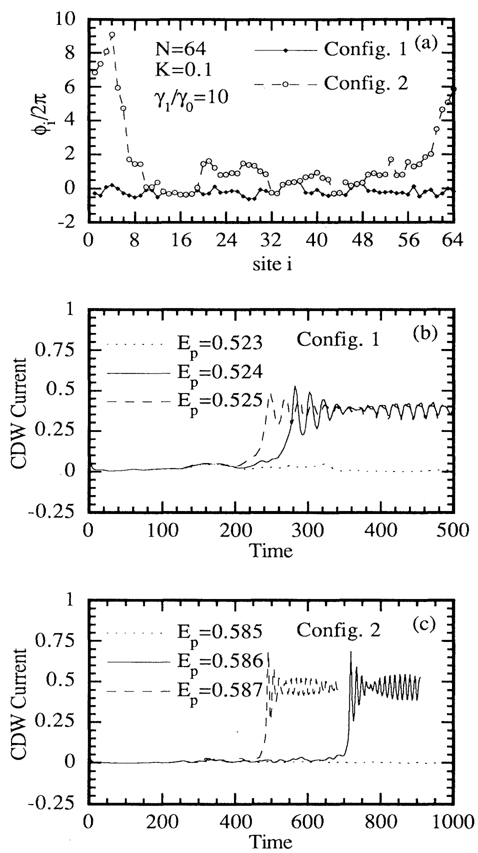

FIG. 12. Numerical simulations of Eq. (4.8) for two different initial configurations. Time is expressed in units of $\gamma_0 \equiv 1$. Current $\dot{\phi}$ is dimensionless. (a) Plot of two initial configurations. For configuration 1, the CDW is in a relaxed state of minimum strain energy, obtained by letting the CDW relax from ϕ_i=0 at $t = -\infty$. For configuration 2, the CDW was allowed to relax to a metastable condition after a pulse (which did not switch) with E_p= 0.523. (b) Current versus time for three values of E_p for configuration 1. At E_p=0.523, the CDW remains pinned, but slides after a delay τ=270 for E_p=0.524 and τ=250 for E_p=0.525. (c) Current versus time for three values of E_p for configuration 2. Note the change in time scale. At E_p=0.585, the CDW remains pinned, but slides after a delay τ=700 for E_p=0.586 and τ=475 for E_p=0.587.

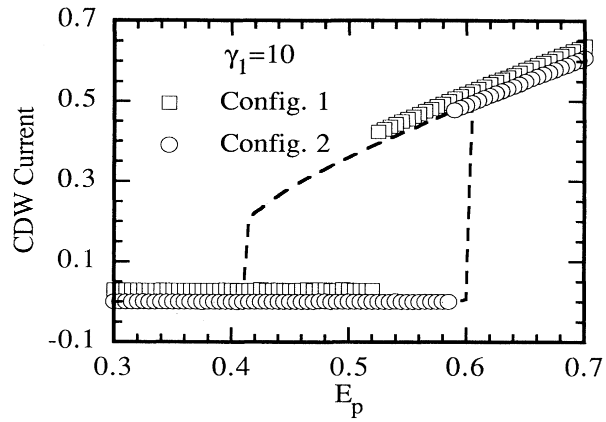

FIG. 13. Final CDW current versus pulse height E_p for configurations 1 and 2 and γ_1=10. The current for configuration 1 is shifted slightly for clarity. The transition to the sliding state occurs at a smaller value of E_p for the unpolarized state. E_p is dimensionless [see Eq. (4.8)].

The threshold for conduction E_p^{th} depends on the initial configuration. Figure 13 shows a plot of the final CDW current versus E_p for configurations 1 and 2. The current for configuration 1 is offset slightly for clarity. The dashed line represents the hysteretic I-V curve obtained by slowly ramping the field E. Just as was seen experimentally in Fig. 9, E_p^{th} is much smaller for configuration 1 where the CDW is unpolarized, than for configuration 2, where the CDW is initially polarized.

We have also examined switching behavior in Eq. (4.8) as a function of γ_1, the normal carrier resistance. Figure 14 shows a plot of the current versus time for three values of γ_1 for the unpolarized initial condition shown in Fig. 12(a). Not shown in this figure is a small initial polarization current which is independent of γ_1. The current quickly drops to almost zero after that and remains small until $t = \tau$, when the current switches on. At the switch, the current oscillations are quite large and the current has been averaged over several oscillation peri-

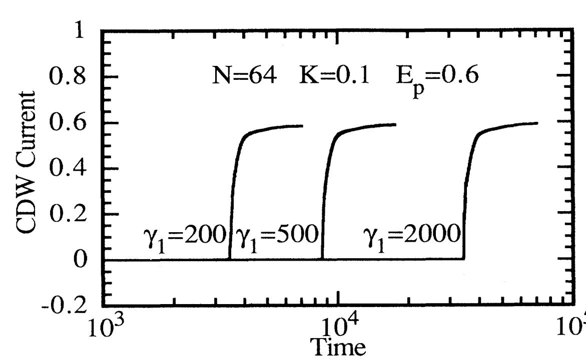

FIG. 14. CDW current response to a pulse $E_p = 0.6$ for three different values of γ_1, the normal carrier resistance. The current has been coarse grained in time for clarity (cf. Fig. 17). The three current traces appear shifted by a constant horizontal amount, indicating that both the delay time τ and the switching time t_{sw} are proportional to γ_1.

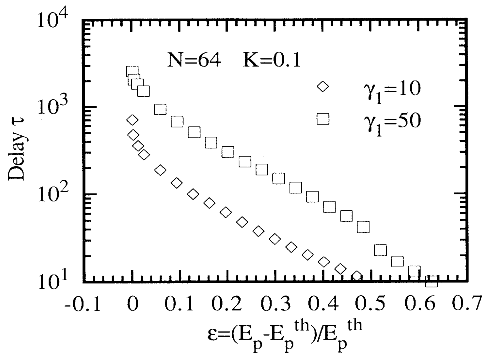

FIG. 15. Plot of delay τ versus reduced pulse height ϵ for two values of γ_1. The initial configuration is a polarized state similar to that shown in Fig. 12. For $\epsilon < 0.02$, τ depends quite sensitively on ϵ. Above $\epsilon = 0.02$, the decrease in τ is much less rapid, although still approximately exponential. For γ_1=50, there is a discontinuous jump near $\epsilon = 0.5$, corresponding to the condition $|\Psi(t=0)| = E_p$.

ods for the sake of clarity [cf. Fig. 17(b)]. It takes a time $t_{\rm sw}$ for the current to reach a maximum. As one can see from Fig. 14, both τ and $t_{\rm sw}$ are proportional to γ_1.

The dependence of the delay τ on $\epsilon \equiv (E_p - E_p^{\rm th})/E_p^{\rm th}$ is shown in Fig. 15. Very close to $\epsilon = 0$, τ depends quite sensitively on ϵ, becoming less so for $\epsilon \geq 0.05$. As one can see, τ drops roughly exponentially as ϵ is increased, similar to that seen experimentally (cf. Fig. 4). The dependence is more closely exponential for $\gamma_1 = 50$ than for $\gamma_1 = 10$.

V. ANALYSIS AND DISCUSSION

A. Origin of delayed conduction

In trying to understand why delayed conduction is observed at all in Eq. (4.8), it is useful to define a complex order parameter

$$\Psi \equiv re^{i\theta} \equiv \frac{1}{N}\sum_{j=1}^{N} e^{i(\phi_j-\beta_j)} \equiv \frac{1}{N}\sum_{j=1}^{N}\psi_j \ . \tag{5.1}$$

The order parameter is represented graphically in Fig. 16.

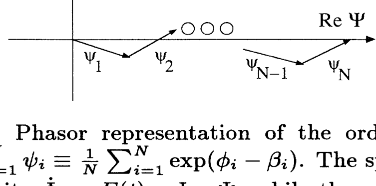

FIG. 16. Phasor representation of the order parameter $\Psi = \frac{1}{N}\sum_{i=1}^{N}\psi_i \equiv \frac{1}{N}\sum_{i=1}^{N}\exp(\phi_i - \beta_i)$. The space-averaged CDW velocity $\dot\Phi = E(t) - \text{Im}\ \Psi$, while the pinning energy $V_{\rm pin} = -\text{Re}\ \Psi$. In the $E=0$ pinned state, Im $\Psi = 0$ *exactly*, and for strong pinning $|\Psi| \approx 1$.

The spatially averaged pinning energy $E_{\rm pin}$ and pinning force $F_{\rm pin}$ are given in terms of Ψ by

$$U_{\rm pin} = -r\cos(\theta) \ , \tag{5.2a}$$

$$F_{\rm pin} = -r\sin(\theta), \tag{5.2b}$$

whereas the CDW current is given by

$$\gamma_0\langle\dot\phi_k\rangle_k = E(t) + F_{\rm pin} = E(t) - r\sin(\theta) \ , \tag{5.3}$$

and is well approximated by $\langle\dot\phi_k\rangle_k \approx \dot\theta$ when $\gamma_1 \gg \gamma_0$, for reasons which will become clear below. We shall consider the case of strong pinning ($K \ll 1$), which is both conceptually simpler and the case we have considered in our simulations. In the $E=0$ pinned state, $U_{\rm pin}$ will be minimized, which means that $r \approx 1$, or $\phi_j - \beta_j \approx 0 = \theta$ for all j.

If the normal carrier resistance γ_1 is much larger than the intrinsic CDW damping γ_0, then there is a separation of time scales for the rigid translation of the CDW and the motion of internal degrees of freedom. However, there is an important coupling between the two, and it is this coupling which leads to conduction delays. To see why this is so, we define new variables Φ and η_j, which correspond to the rigid translation of the CDW and to the motion of internal degrees of freedom, respectively:

$$\Phi \equiv \langle\phi_k\rangle_k \ , \tag{5.4a}$$

$$\eta_j \equiv \phi_j - \Phi \ . \tag{5.4b}$$

The equations of motion for these new variables can be found from Eq. (4.8):

$$\gamma_0\dot\Phi = -r\sin(\theta) + E(t) \ , \tag{5.5a}$$

$$(\gamma_0+\gamma_1)d_j\dot\eta_j = K\Delta\eta_j - \sin(\eta_j - \beta_j + \Phi) + d_j r\sin(\theta) \ . \tag{5.5b}$$

One can find the equation of motion for the magnitude and phase of the order parameter Ψ:

$$\dot\theta = \frac{1}{N}\sum_{j=1}^{N}\frac{1}{r}\cos(\eta_j - \beta_j + \Phi - \theta)\dot\eta_j + \dot\Phi \ , \tag{5.6}$$

$$\dot r = \frac{1}{N}\sum_{j=1}^{N} -\sin(\eta_j - \beta_j + \Phi - \theta)\dot\eta_j \ . \tag{5.7}$$

By combining Eqs. (5.5a) and (5.6), one sees that when the pulse is turned on, the CDW behaves like a single-degree-of-freedom damped driven pendulum:

$$\gamma_0\dot\theta = E_p - r(t)\sin(\theta) + O(\gamma_0/\gamma_1). \tag{5.8}$$

The initial polarization of the CDW is brief, and after a time $t \sim \gamma_0$ the CDW current drops almost to zero. The internal degrees of freedom move on a time scale γ_1. For now, let us consider the case in which the CDW is initially unpolarized. Then, one can ignore the elastic contributions, and the η_j obey the approximate equation

$$\begin{aligned}(\gamma_0+\gamma_1)\dot\eta_j &\approx r\sin(\theta) - \sin(\eta_j - \beta_j + \Phi)/d_j \\ &\approx E_p - \sin(\eta_j - \beta_j + \Phi)/d_j \ .\end{aligned} \tag{5.9}$$

The η_j for which $d_j > 1$ will be above "threshold" and will advance, while the η_j for which $d_j < 1$ will remain "pinned" and will in fact move slightly in the opposite direction, due to the value of Φ. The net result is that the magnitude r will decrease due to dephasing of the order parameter. This dephasing occurs on a time scale γ_1. As r decreases, the effective threshold in Eq. (5.8) decreases, and when $r \approx E$, the CDW switches. Even when the CDW begins to slide, there is still a bottleneck because r is still comparable to E. The steady state is characterized by $r \approx 0$, and takes a time $t_{\rm sw} \propto \gamma_1$ to approach that state. Hence both τ and $t_{\rm sw}$ are proportional to γ_1.

The motion of the order parameter Ψ is shown graphically in Fig. 17(a) for a numerical simulation in which γ_1=50 and $E_p = 0.6$. The dashed line corresponds to $\mathrm{Im}\Psi = E_p = 0.6$. At point A, $t = 0$ and the current $\dot{\Phi} = 0.6$. The order parameter Ψ moves in a circular arc towards point B, which is reached at $t = 6$. The dynamics are very slow as Ψ creeps along the dashed line, and at $t = 933$ the current has reached point C. The peak of the first current oscillation occurs at point D at $t = 945$. The corresponding CDW current is plotted versus time in Fig. 17(b). The current oscillations are quite large when the CDW switches because r is still large. The fact that the current oscillations are large is an artifact of the equations of motion in one spatial dimension. Oscillations are not expected to be large in higher dimensions.

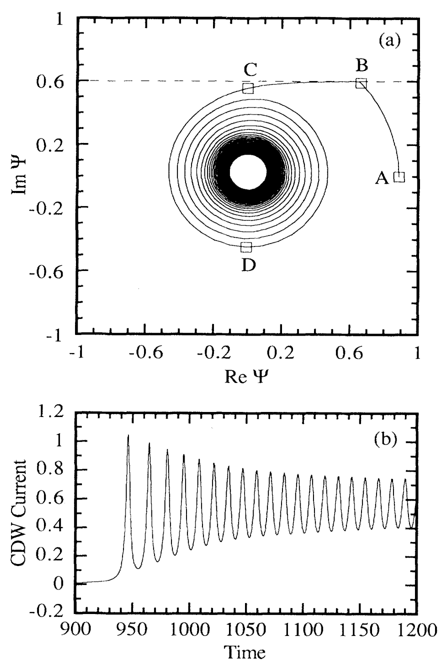

FIG. 17. (a) "Configuration-space" plot of $\Psi(t) = r(t)\exp[i\theta(t)]$ for $\gamma_1/\gamma_0 = 50$, and E_p=0.6, beginning from a polarized configuration. The dashed line corresponds to $\mathrm{Im}\Psi = E_p$. The CDW current is given by $\gamma_0\langle\dot{\phi}_k\rangle_k = E_p - \mathrm{Im}\Psi$. The CDW begins at point A at $t = 0$ in a state of minimum pinning energy, with $\Psi(t = 0)$=0.88. When the pulse is turned on, θ increases with r essentially constantly until Ψ approaches the dashed line at point B. At this point the velocity is nearly zero. Because of the distribution of impurity domain sizes d_j, the ψ_j begin to dephase, and r decreases at a rate $\propto \gamma_1$. Near point C, $r \approx E_p$, and the CDW can begin to slide quasirigidly and $\Psi(t)$ spirals in toward $r \approx 0$. The peak of the first current oscillation occurs at point D. (b) Plot of CDW current for same conditions as in (a). The current increases abruptly near $t = 940$. The current oscillations are large near the beginning of the switch because $|\Psi(t)| \approx E_p$, and the CDW is behaving like a single degree of freedom oscillator near theshold.

B. Dependence on initial configuration

It was seen both experimentally and numerically that the threshold for conduction depended sensitively on the initial configuration. Experimentally, the threshold voltage $V_p^{\rm th}$ was lower if the CDW configuration was prepared either by heating the CDW above the Peierls transition or by polarizing it in the opposite direction. Numerically, we observe a similar dependence on initial configuration. If the CDW begins in a polarized configuration, then the amount of dephasing of Ψ will be much smaller because the "local fields" which cause the η_j to move at different velocities in Eq. (5.5b) will be counterbalanced by elastic forces, and the threshold field will increase as a result.

Experimentally, the polarization currents were much larger when the initial configuration was prepared by heating the CDW above T_P than by driving the CDW with a pulse of the opposite sign. The excess current seen in the heating experiments may be due to a weak temperature dependence in the CDW wave vector Q. This hypothesis is consistent with a small shift in the CDW wave vector observed by x-ray diffraction, depending on whether the CDW was cooled in zero electric field or driven above threshold.[38] This effect cannot be modeled using closed boundary conditions, but presumably could if one employed open boundary conditions.

C. Pulse-height dependence

The dependence of τ on pulse height agrees well between experiment and theory. In both cases one sees roughly two regions: for very small reduced field ϵ there is a very sensitive dependence of τ on ϵ, whereas for larger ϵ the delay τ decreases approximately exponentially with ϵ. We have not tried to find numerically the distribution of delays versus ϵ because that would require knowing the distribution of initial configurations, but we do expect a more sensitive dependence of τ on initial configuration near the threshold. The threshold itself depends on the initial configuration, as was discussed in Sec. V B.

D. Temperature dependence

The temperature dependence of the average delay τ and the switching time $t_{\rm sw}$ were both found to be activated with an activation energy E_a comparable to the CDW gap. Numerically, it was found that both τ and

t_{sw} were proportional to γ_1, where γ_1 is interpreted as the resistance due to uncondensed carriers. In a semiconducting CDW, one would expect γ_1 to be activated. In order for the numerical simulations to be consistent with experiment, one must assume that

$$\gamma_1 \propto \exp(E_a/k_BT). \tag{5.10}$$

In $NbSe_3$, however, the Fermi surface is not completely gapped, and hence contributions to the Ohmic conductivity come from both quasiparticles excited across the CDW gap and from ungapped electrons. Below $T =$ 48 K the resistance in $NbSe_3$ *decreases* with temperature, while the hysteresis in the I-V curves *increases.* Although it appears difficult to justify microscopically, the evidence is quite compelling that the ungapped electrons in $NbSe_3$ do not play a significant role in screening CDW fluctuations.[14,29]

The remarkable qualitative agreement between the experimental results and numerical simulations provides strong evidence that the mechanism for switching in $NbSe_3$ is governed by the interaction between the CDW and uncondensed carriers. However, assumption 5.10 is clearly at odds with the fact that $NbSe_3$ is metallic at low temperatures. The mounting body of evidence consistent with this assumption impels us to search for a microscopic description.

ACKNOWLEDGMENTS

We acknowledge useful discussions from J. Carlson, S. N. Coppersmith, P. B. Littlewood, and A. Montakhab. This work was supported by the National Science Foundation Grant No. DMR 9214995 (J.L. and M.S.S.), the Alfred P. Sloan Foundation (M.S.S.), and INCOR (J.L.). Computations were performed in part at the San Diego Supercomputer Center.

[1] For a review of the dynamics of sliding charge-density waves, see *Charge Density Waves in Solids*, edited by L. P. Gorkov and G. Grüner, Modern Problems in Condensed Matter Sciences Vol. 25 (North-Holland, Amsterdam, 1989).

[2] H. Fukuyama and P. A. Lee, Phys. Rev. B **17**, 535 (1978); P. A. Lee and T. M. Rice, *ibid.* **19**, 3870 (1979).

[3] R. M. Fleming *et al.*, Phys. Rev. B **33**, 5450 (1986).

[4] R. J. Cava *et al.*, Phys. Rev. Lett. **53**, 1677 (1984).

[5] A. Maeda, T. Furuyama, and S. Tanaka, Solid State Commun. **55**, 951 (1985).

[6] A. Maeda, T. Furuyama, K. Uchinokura, and S. Tanaka, Physica B **143**, 123 (1986).

[7] L. Mihály and G. X. Tessema, Phys. Rev. B **33**, 5858 (1986).

[8] G. Mihaly and P. Beauchene, Solid State Commun. **63**, 911 (1987).

[9] L. Sneddon, Phys. Rev. B **29**, 719 (1984).

[10] P. B. Littlewood, Solid State Commun. **65**, 1347 (1988).

[11] For a review of the dynamics of switching CDW's, see R. P. Hall, M. F. Hundley, and A. Zettl, Phys. Rev. B **38**, 13 002 (1988); R. P. Hall and A. Zettl, *ibid.* **38**, 13 019 (1988); M. S. Sherwin, A. Zettl, and R. P. Hall, *ibid.* **38**, 13 028 (1988), and references therein.

[12] M. Inui, R. P. Hall, S. Doniach, and A. Zettl, Phys. Rev. B **38**, 13 047 (1988).

[13] R. P. Hall, M. S. Sherwin, and A. Zettl, Phys. Rev. B **29**, 7076 (1984).

[14] J. Levy, M. S. Sherwin, F. F. Abraham, and K. Wiesenfeld, Phys. Rev. Lett. **68**, 2968 (1992).

[15] R. P. Hall and A. Zettl, Solid State Commun. **50**, 813 (1984).

[16] M. S. Sherwin, A. Zettl, and R. P. Hall, Phys. Rev. B **38**, 13 028 (1988).

[17] J. Levy, M. S. Sherwin, and J. Theiler, Phys. Rev. Lett. **70**, 2957 (1993).

[18] A. Zettl and G. Grüner, Phys. Rev. B **26**, 2298 (1982).

[19] G. Kriza, A. Janossy, and G. Mihaly, in *Charge-Density Waves in Solids*, edited by G. Hutiray and J. Sólyom, Lecture Notes in Physics Vol. 217 (Springer-Verlag, Berlin, 1984), p. 426.

[20] B. Joos and D. Murray, Phys. Rev. B **29**, 1094 (1984).

[21] S. H. Strogatz and R. M. Westervelt, Phys. Rev. B **40**, 10 501 (1989).

[22] J. Levy and M. S. Sherwin, Phys. Rev. B **43**, 8391 (1991).

[23] J. Levy and M. S. Sherwin (unpublished).

[24] K. Wiesenfeld and M. Sherwin, Phys. Rev. A **45**, 3467 (1992).

[25] P. Colet and K. Wiesenfeld, Phys. Rev. A **46**, 4676 (1992).

[26] W. A. Challener and P. L. Richards, Solid State Commun. **52**, 117 (1984).

[27] A. Fournel *et al.*, Physica B **143**, 177 (1986).

[28] R. V. Coleman *et al.*, Appl. Surf. Sci. **60**, 485 (1992).

[29] T. L. Adelman *et al.*, Phys. Rev. B **47**, 4033 (1993).

[30] R. P. Hall, M. F. Hundley, and A. Zettl, Phys. Rev. B **38**, 13 002 (1988).

[31] Large lattice defects can be ultrastrong pinning centers. See K. Svoboda, A. Zettl, and M. S. Sherwin, Solid State Commun. **70**, 859 (1989).

[32] S. H. Strogatz, C. M. Marcus, R. M. Westervelt, and R. E. Mirollo, Phys. Rev. Lett. **61**, 2380 (1988).

[33] A. Jánossy, G. Mihály, and L. Mihály, in *Charge-Density Waves in Solids* (Ref. 19), p. 412.

[34] W. Wonneberger and H. J. Breymayer, Z. Phys. B **56**, 241 (1984).

[35] P. B. Littlewood, Phys. Rev. B **33**, 6694 (1986).

[36] L. Pietronero and S. Strässler, Phys. Rev. B **28**, 5863 (1983).

[37] This ansatz differs slightly from that of Pietronero and Strässler (Ref. 36), who assume that the damping only occurs at the impurity sites. This assumption allows the equations of motion to be discretized *exactly*, yielding the following equation of motion: $\gamma_0\dot{\phi}_j = K\Delta^2\phi_j + \sin(\phi_j - \beta_j) + d_jE$. This equation gives unphysically large strains for large E.

[38] R. E. Thorne (private communication).